ACS OMEGA

Open Access

http://pubs.acs.org/journal/acsodf

Article

Highly Efficient Adsorption of Norfloxacin by Low-Cost Biochar: Performance, Mechanisms, and Machine Learning-Assisted Understanding

Miaomiao Zhang,[§] Pengwei Li,[§] Dong Guo, Ziheng Zhao, Weisheng Feng, and Zhijuan Zhang*

Cite This: *ACS Omega* 2024, 9, 30813−30825

Read Online

ACCESS | Metrics & More | Article Recommendations | Supporting Information

ABSTRACT: This study employed potassium carbonate (K_2CO_3) activation using ball milling in conjunction with pyrolysis to produce biochar from one traditional Chinese herbal medicine *Atropa belladonna* L. (ABL) residue. The resulting biochar KBC_{800} was found to possess a high specific surface area (S_{BET} = 1638 m^2/g) and pore volume (1.07 cm^3/g), making it effective for removing norfloxacin (NOR) from wastewater. Batch adsorption tests confirmed its effectiveness in eliminating NOR, along with its excellent resistance to interference from impurity ions or antibiotics. Notably, the maximum experimental NOR adsorption capacity on KBC_{800} was 666.2 mg/g at 328 K, surpassing those of other biochar materials reported. The spontaneous and endothermic adsorption of NOR on KBC_{800} could be better suited to the Sips model. Additionally, KBC_{800} adsorbs NOR mainly by pore filling, with electrostatic attraction, $\pi-\pi$ EDA interactions, and hydrogen bonds also contributing significantly. The machine learning model revealed that NOR adsorption on the biochar was significantly affected by the initial concentration, followed by S_{BET} and average pore size. Based on the random forest model, it is demonstrated that biochar is able to adsorb NOR effectively. It is noteworthy that the use of low-cost pharmaceutical wastes to produce adsorbents for emerging contaminants such as antibiotics could have greater potential for future practical applications under the ongoing dual carbon policy.

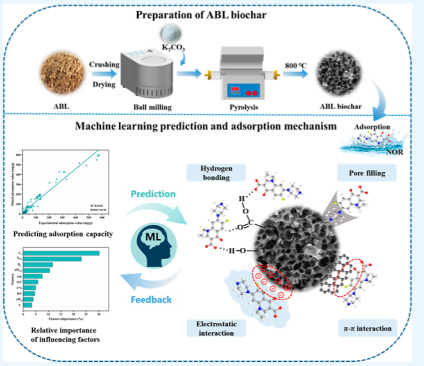

1. INTRODUCTION

Both humans and animals have relied heavily on antibiotics to treat a variety of ailments, and their ultimate fate in the environment has attracted considerable attention for a number of years.[1,2] Approximately 70% of the antibiotics that are not completely metabolized are excreted into wastewater through urine and feces and can potentially enter the human drinking water supply through the water cycle, thereby posing a significant threat to both aquatic ecosystems and human well-being.[3,4] In China, the annual consumption of antibiotics, particularly norfloxacin (NOR), a broad-spectrum fluoroquinolone antibiotic known for its favorable pharmacokinetic properties and potent antibacterial activity, reaches hundreds of tons.[5] Despite its widespread use, the escalating levels of NOR residues in aquatic environments pose a growing concern. The persistence of NOR in water systems heightens the likelihood of antibiotic resistance, thereby compromising human immune function and exacerbating allergic responses.[6] Consequently, cost-effective and environmentally friendly water treatment technologies to enhance NOR elimination are urgently needed and has become one of the major challenges.

Presently, the treatment technologies commonly employed for NOR and other antibiotics include adsorption,[7] biological treatment,[8] oxidation processes,[9] and membrane filtration.[10] Thereinto, the adsorption technique has gained significant attention because of its efficiency, simplicity, cost-effectiveness, and nontoxic nature.[11] Various materials, such as carbon-based materials,[12] bentonite-chitosan composite,[13] hydrogel,[14] MOFs,[15] and zeolite molecular sieves,[9] can be utilized in the adsorption process. A particularly effective adsorbent in the antibiotic removal process is biochar (BC) owing to its large surface area, abundance of surface functional groups, and developed pores.[16] Guy Laurent Zanli et al.[11] synthesized a N-doped biochar from cocoa shell, and they demonstrated a Langmuir NOR adsorption capacity of 133.5 mg/g with a contact time of 72 h. Wang et al.[17] prepared a loofah activated carbon-loaded agarose aerogel and presented a Langmuir NOR adsorption capacity of 434.8 mg/g with an equilibrium time of 140 h. These adsorbents demonstrate deficiencies in terms of low NOR adsorption capacity, inadequate adsorption efficiency, and prolonged adsorption equilibrium time. Thus, it is crucial to create an adsorbent that can efficiently eliminate environmental contaminants on a vast scale in order to advance adsorption technology.

Received: April 11, 2024
Revised: June 14, 2024
Accepted: June 27, 2024
Published: July 5, 2024

Chinese herbal medicine (CHM) is widely utilized in diverse applications, leading to substantial residues that have emerged as a predominant wastes stream in China. *Atropa belladonna* L. (ABL), a well-known traditional CHM, is commonly used for the management of gastrointestinal colic and the alleviation of symptoms including excessive sweating, salivation, bradycardia, vertigo, and syncope.[18] The Henan Province serves as an ABL planting base encompassing 3000 acres, from which harvested ABL is supplied to local pharmaceutical factories for the production of analgesic plasters. The substantial quantity of ABL residue remaining contains lignin, cellulose, hemicellulose, as well as various functional groups such as carboxyl and hydroxyl groups, rendering it a valuable precursor for biochar synthesis.[19] Despite the broad applicability of biochar derived from ABL, the majority of current BC adsorbents necessitate the utilization of multistep chemical activation using acids, alkali, or inorganic salts. Among those chemical activation reagents, K_2CO_3 is a milder activator due to its nontoxicity, weak corrosivity, and environment-friendliness.[20] In the activation process, K_2CO_3 plays a dual role by facilitating pore formation through alkaline erosion and generating new micropores as a result of reactions with carbon at elevated temperatures.[21] Additionally, most studies only evaluated the impact of a single variable on NOR adsorption performance of BC, and the introduction of machine learning (ML) effectively solves the challenge of assessing the relative importance of each influential factor and their combined effects on the material properties.[22,23]

Herein, our research demonstrated that ABL biochar can be synthesized effectively with a large surface area and oxygen-rich functional groups. The present research was designed with the aim of investigating the optimal adsorption performance of the prepared ABL biochar through batch adsorption experiments (kinetics, isotherms, and thermodynamics). The surface physicochemical properties of the obtained ABL biochar were characterized. Besides, the mechanism of NOR adsorption on the ABL biochar was scrutinized. Furthermore, random forest (RF) was applied to build the prediction model for evaluating the NOR adsorption on the prepared biochar. Additionally, the model incorporates the material properties and adsorption conditions, allowing for a comprehensive evaluation of the relative importance and influence of each variable on NOR adsorption capacity. Such findings hold considerable importance in guiding the treatment of real-world wastewater and polluted groundwater contaminated with NOR.

2. MATERIAL AND METHODS

2.1. Chemicals and Materials. Traditional Chinese medicine residue (*A. belladonna* L, ABL) came from a traditional Chinese medicine factory in Henan. Norfloxacin (NOR) ($C_{16}H_{18}FN_3O$), oxytetracycline (OTC) ($C_{22}H_{24}O_9N_2$), penicillin-G (PEN-G) ($C_{16}H_{17}KN_2O_4S$), erythromycin (ERY) ($C_{37}H_{67}NO_{13}$), sulfadiazine (SUL) ($C_{10}H_{10}N_4O_2S$), HCl, NaOH, Na_2SO_4, Na_2CO_3, $NaHCO_3$, NaCl, KCl, $MgCl_2$, and $CaCl_2$ were bought from J&K Scientific. These reagents are all analytical grade and used without further operations.

2.2. Synthesis of Adsorbents. 2 g of ABL and 2 g of K_2CO_3 were mixed in a ball mill for 20 min to produce the KB. The KB was then heated in a tube furnace under N_2 gas at temperatures of 600, 700, and 800 °C, respectively, with a heating rate of 5 °C/min. Heating at each temperature lasted for 1 h before KB was cooled to room temperature in order to produce a series of biochar products. Afterward, pyrolysis products were extracted, washed with deionized water to neutral pH, filtered, and dried. These samples were named KBC_{600}, KBC_{700}, and KBC_{800}. The ball-milled ABL sample was carbonized at 800 °C for 1 h, then washed, dried, and ground; it was designated as BC_{800}. In the above samples, "K" represents "K_2CO_3", "B" represents the ball milling process, "C" represents the carbonization behavior, and 600, 700, and 800 represent the corresponding carbonization temperatures. The characterization method of the ABL biochar is detailed in Text S1.

2.3. Batch Adsorption Studies for NOR. A batch experiment was conducted to investigate the effects of initial pH (2−12), adsorbent dosage (0.2−1.0 g/L), adsorption time (0−1440 min), interfering ions (Ca^{2+}, Mg^{2+}, K^+, Na^+, SO_4^{2-}, CO_3^{2-}, and HCO_3^-) at concentrations of 1 and 100 mmol/L, as well as the impact of interfering antibiotics (ERY, OTC, PEN-G, and SUL) at concentrations of 10 and 100 mg/L on NOR adsorption. It was found that NOR measurement was not affected by the presence of other antibiotics. In the aforementioned experiments, alongside variations in pH levels, solutions of HCl and NaOH with concentrations ranging from 0.1 to 1.0 mol/L were utilized for pH adjustment to a target of 7.0 ± 0.05. Following the attainment of adsorption equilibrium, the final solution exhibited a measured pH value of 7.14 ± 0.05. Furthermore, in investigations pertaining to the impact of initial NOR concentration (ranging from 25 to 400 mg/L) on adsorption capacity, as well as adsorption isotherm and the thermodynamic analysis at temperatures of 298, 308, 318, and 328 K, the pH of the adjusted solution was maintained at 6.3 ± 0.05. After reaching the adsorption equilibrium, the final pH of the solution was 6.42 ± 0.05.

In experiments with competitive substances, 5 mg of adsorbent was added to 10 mL of a 100 mg/L NOR solution. Each adsorption experiment was repeated three times under identical conditions. The concentration of residual NOR was determined using a UV−vis spectrophotometer (U-3900H, Hitachi) at 273 nm. The adsorption capacity and removal rate of NOR were determined using the following eqs 1 and 2.

$$q_e = \frac{(C_0 - C_e)V}{m} \tag{1}$$

$$R = \frac{(C_0 - C_e)}{C_0} \times 100\% \tag{2}$$

where q_e (mg/g) and R (%) are separately the equilibrium adsorption capacity and removal rate of NOR; C_0 (mg/L) and C_e (mg/L) are separately the initial NOR concentrations and equilibrium concentration; m (g) is the adsorbent dosage; and V (L) is the NOR solution volume.

The adsorption kinetics, isotherms, and thermodynamics are calculated using the equations provided in Table S1.

2.4. Regeneration Performance. The experiment involved maintaining an NOR concentration of 100 mg/L and a KBC_{800} dosage of 0.5 g/L. In each cycle, the KBC_{800} biochar with adsorbed NOR was soaked with 1 M NaOH and a series of purification steps such as continuous magnetic stirring and rinsing with deionized water. After overnight in the oven, the recovered biochar was used to explore its reusability and stability in the next cycle. The desorption rate of NOR on KBC_{800} is determined by eq 3.

$$D\% = \frac{(C_d V_d)}{(C_0 - C_e)V} \times 100\% \tag{3}$$

https://doi.org/10.1021/acsomega.4c03496
ACS Omega 2024, 9, 30813−30825

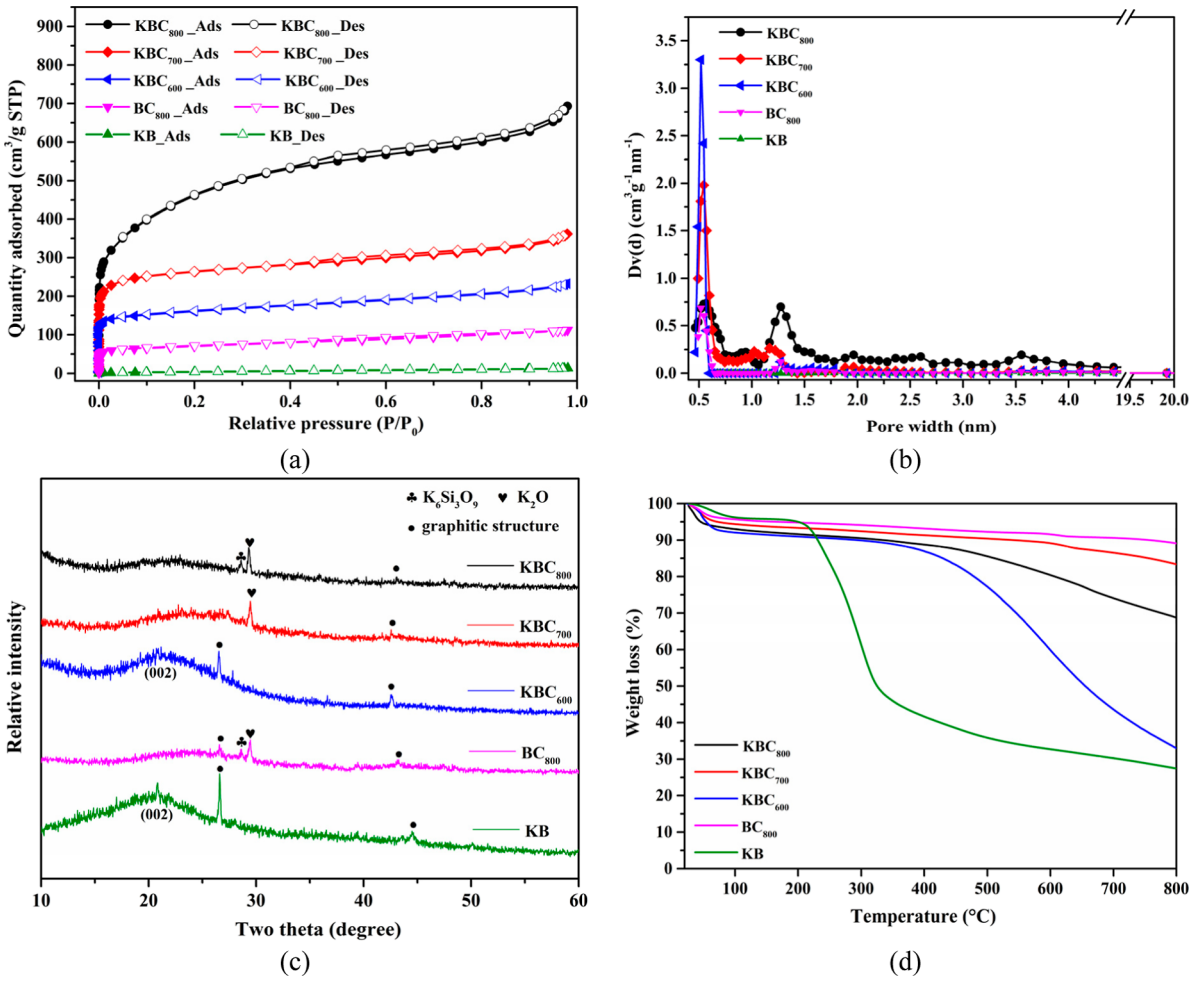

Figure 1. (a) N_2 adsorption−desorption isotherm, (b) nonlocal density functional theory pore size distribution, (c) XRD patterns, and (d) TGA profiles of ABL biochar.

Table 1. Pore Characteristics of ABL Biochar[a]

samples	S_{BET} (m^2/g)	S_{Micro} (m^2/g)	S_{Meso} (m^2/g)	$S_{Langmuir}$ (m^2/g)	V_{Micro} (cm^3/g)	V_{Total} (cm^3/g)	average pore diameter (nm) (NLDFT)
KBC_{800}	1638	1086	552.0	2327	0.4950	1.072	2.617
KBC_{700}	1007	813.6	193.2	1196	0.3250	0.5588	2.219
KBC_{600}	605.3	460.2	144.8	741.1	0.1789	0.3603	2.381
BC_{800}	257.2	88.37	168.4	335.8	0.06900	0.1688	2.692
KB	16.98	9.325	8.421	28.24	NA	0.02120	4.943

[a]NA: not available.

where D (%) is the desorption ratio, C_d (mg/L) is the concentration of NOR in the desorption solutions, V_d is the volume of the desorption solution (mL); V, C_0, and C_e are the same as those defined earlier.

2.5. Machine Learning. In order to establish an ML model suitable for evaluating the performance of biochar and AC materials in removing NOR, the experimental data of NOR adsorption on AC and BC materials were collected from a total of 18 journal publications in the last 7 years. By carefully reviewing the experimental data provided by these sources, 144 sets of relevant data for 44 adsorbents were obtained[6,11,17,24−38] (Table S2). The input data for the ML modeling had 10 descriptors, encompassing 7 descriptors for the adsorbents (S_{BET} in m^2/g, D_p in nm, pH_{pzc}, C %, H/C, O/C and ash %), 2 descriptors for the adsorption conditions (T and pH_{sol}), and the ratio of initial NOR concentration to BC dose (C_0 in mg/g). During the training of ML model, to prevent possible data leakage in the data-splitting process, the group selection approach was selected. The group labels can be found in Table S3. These data sets were then divided into training and test sets in a 7:3 ratio for the purpose of constructing ML models. Furthermore, a 5-fold cross-validation of the RF model was conducted to avoid the model overfitting. Through repeated experimental evaluations, the average value was determined as the final result. A comprehensive analysis was conducted to determine the NOR adsorption capacity on BC (q_e, mg/g) based on 10 key factors encompassing various physicochemical properties and adsorption environments. More detailed information can be found in the Supporting Information (Text S2).

https://doi.org/10.1021/acsomega.4c03496
ACS Omega 2024, 9, 30813−30825

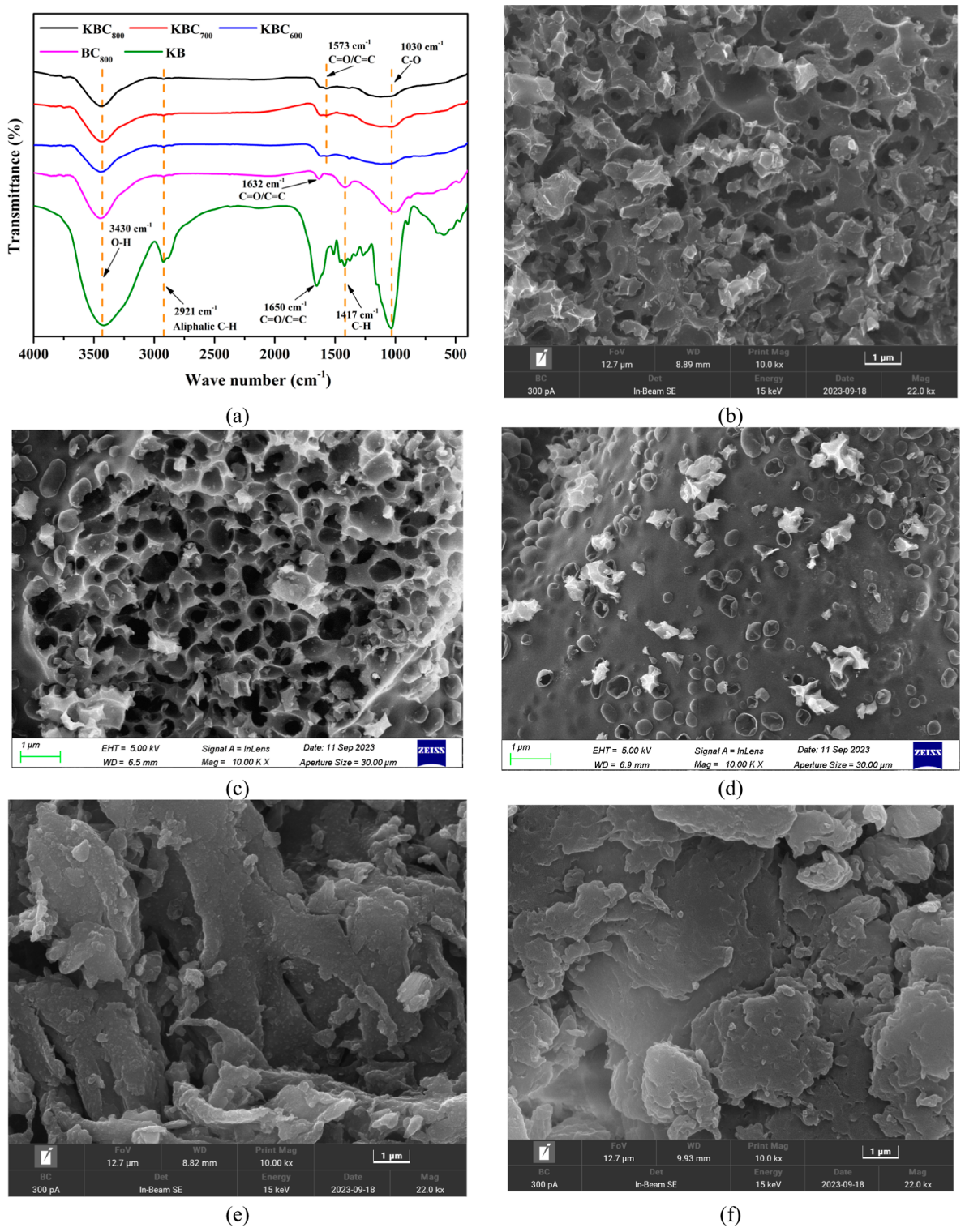

Figure 2. FTIR spectra of ABL biochar materials (a) and SEM patterns, KBC_{800} (b), KBC_{700} (c), KBC_{600} (d), BC_{800} (e), and KB (f).

3. RESULTS AND DISCUSSION

3.1. Characterization of Biochar. Figure 1a displays the N_2 adsorption−desorption isotherms at 77 K of the obtained ABL biochar. KB exhibits a low N_2 adsorption capacity at very low relative pressures, with minimal changes as the relative pressure increases. The surface porosity of KB is extremely low, with an S_{BET} value of only 16.98 m^2/g, representing the mixture nature of K_2CO_3 and ABL residue. In contrast, KBC_{800}, KBC_{700}, and KBC_{600}, display typical type-I isotherms with H4 hysteresis loops. The pore size distributions of these samples primarily fall within the range of 0.4−2.5 nm (Figure 1b). The pore size distributions of HK and BJH as shown in Figure S1 provide evidence for the presence of abundant microporous and mesoporous structures. An increase in pyrolysis temperature results in a shift of the pore size distribution toward larger sizes. Specially, a higher pyrolysis temperature range of 600−800 °C leads to an increase in S_{BET} from 605 to 1638 m^2/g and V_{Total}

https://doi.org/10.1021/acsomega.4c03496
ACS Omega 2024, 9, 30813−30825

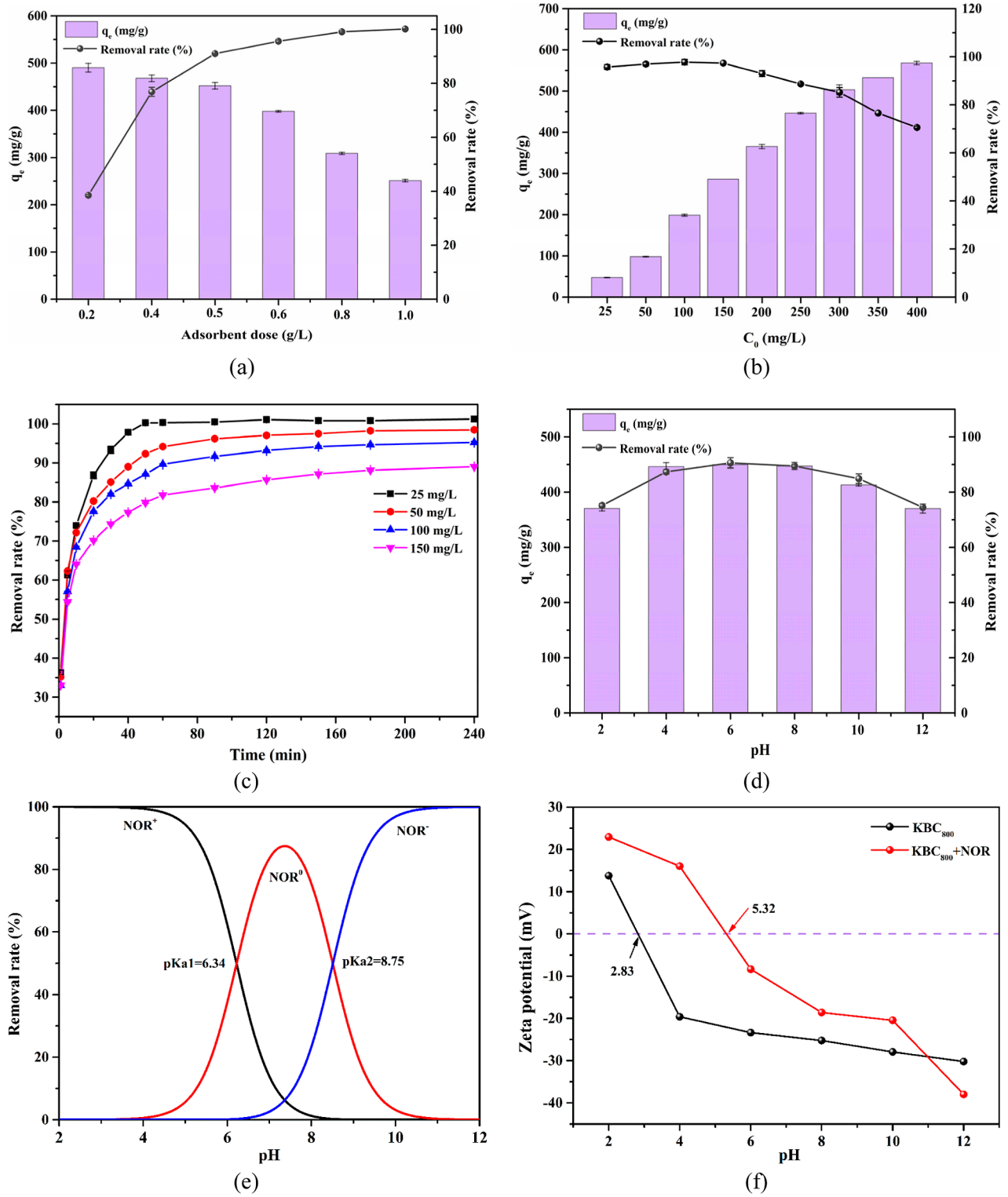

Figure 3. Adsorption performance: the influence of adsorbent dosage (a), initial concentration of NOR (b), adsorption time (c), and the initial pH of the solution (d) on the adsorption capacity and removal efficiency of NOR; ion composition distribution of NOR (e); zeta potential measurement of KBC_{800} and KBC_{800} + NOR (f). [Adsorption conditions: (a) adsorbent dosage 0.2−1.0 g/L, $C_{0,NOR}$ = 250 mg/L, t = 1440 min, T = 25 °C, n = 3; (b) adsorbent dosage 0.5 g/L, $C_{0,NOR}$ = 25−400 mg/L, t = 1440 min, T = 25 °C, n = 3; (c) adsorbent dosage 0.5 g/L, $C_{0,NOR}$ = 25−150 mg/L, t = 240 min, T = 25 °C, n = 3; (d) adsorbent dosage 0.5 g/L, $C_{0,NOR}$ = 250 mg/L, pH = 2−12, t = 1440 min, T = 25 °C, n = 3]. Error bars represent standard deviation.

from 0.36 to 1.07 cm^3/g (Table 1). The development of pore structures is primarily accomplished through etching and the release of gases from the carbon matrix during the activation process. Initially, K_2CO_3 decomposes at elevated temperatures (typically >700 °C) to generate K_2O and CO_2. Subsequently, the carbon matrix interacts with CO_2 to form CO, leading to the creation of micropores.[39] Furthermore, K_2CO_3 and K_2O can also react with the carbon matrix at temperatures exceeding 700 °C, generating gas and enhancing the pore structure.[40] Additionally, BC_{800}, obtained via direct pyrolysis of ABL after

https://doi.org/10.1021/acsomega.4c03496
ACS Omega 2024, 9, 30813−30825

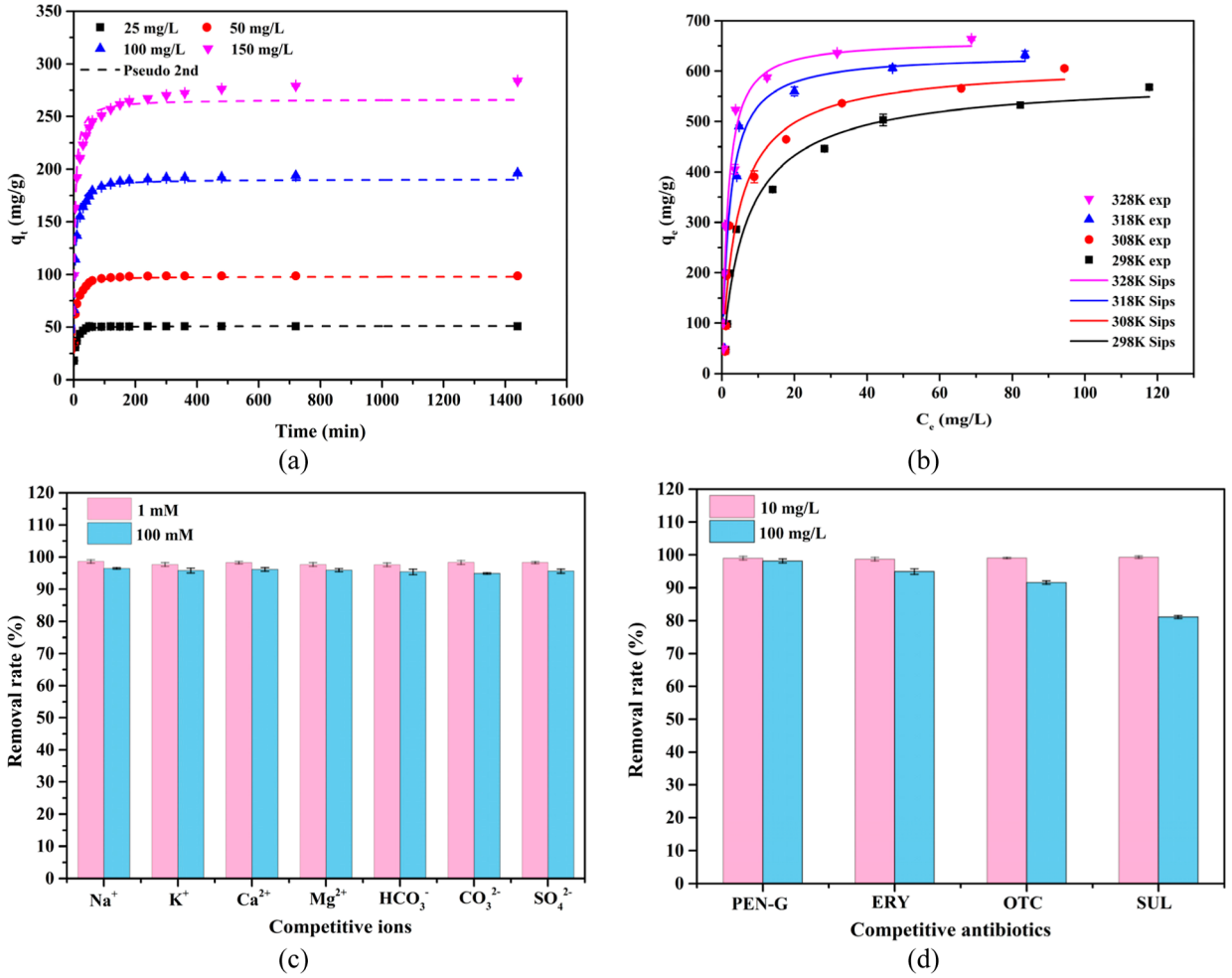

Figure 4. Adsorption kinetics fitting: pseudo-second-order kinetic model (a); adsorption isotherm fitting: sips model (b); influence of interfering ions; (c) and interfering antibiotics (d) in the solution on the removal efficiency of NOR. [Adsorption conditions: (a) adsorbent dosage 0.5 g/L, $C_{0,NOR}$ = 25−150 mg/L, t = 1440 min, T = 25 °C, n = 3; (b) adsorbent dosage 0.5 g/L, $C_{0,NOR}$ = 25−400 mg/L, t = 1440 min, T = 25−55 °C, n = 3; (c,d) adsorbent dosage 0.5 g/L, $C_{0,NOR}$ = 100 mg/L, t = 1440 min, T = 25 °C, n = 3]. Error bars represent standard deviation.

ball milling, exhibits a type-I isotherm in the absence of K_2CO_3. The BET surface area and total pore volume of the samples containing K_2CO_3 are significantly higher than those without K_2CO_3, suggesting that the presence of K_2CO_3 facilitates the formation of a porous structure.[41,42]

Figure 1c shows that KB and KBC_{600} exhibit a large envelope peak (002) within the 20−30° range, along with a broad frequency peak near 43° (100), indicating the presence of graphene within the disordered carbon crystallites.[43−45] When the pyrolysis temperature increases, the peak intensity of KBC_{700} and KBC_{800} at (002) and (100) weakens and the peak shape broadens, demonstrating that the process of high-temperature pyrolysis hinders the formation of amorphous pore walls and facilitates the development of a graphite structure.[41,46] Furthermore, when the pyrolysis temperature reaches a sufficiently high level, the generation of $K_6Si_3O_9$ and K_2O occurs.[39]

The thermal stability of the biochar is depicted in Figure 1d. Except for KB, all other biochar obtained began to decompose at temperatures higher than 450 °C, owing to the gradual breakdown of lignin.[47−49] Notably, KBC_{700}, KBC_{800}, and BC_{800} exhibited no decomposition even at elevated temperatures of 500 °C, indicating excellent thermal stability.

Table S4 shows that high-temperature pyrolysis increases C content and decreases H and O content through reactions like dehydration, decarboxylation, and dihydroxylation.[50] KBC_{800} exhibits the lowest H/C ratio, suggesting the strongest aromaticity. Moreover, the (O + N)/C ratio reveals surface polarity, with lower values indicating weak surface hydrophilicity and polarity in KBC_{800}.[51] Consequently, the hydrogen bonding between biochar and NOR is reduced, while $\pi-\pi$ interactions are enhanced. Meanwhile, excessive ash % is not conducive to the formation of porous structures and the adsorption of pollutants.[52]

Figure 2a illustrates the presence of peaks at specific wavenumbers, namely, 3430 cm^{-1} (corresponding to the O−H stretching vibration of phenol),[53] 2921 cm^{-1} (indicative of stretching vibration of aliphatic C−H bonds), 1632, 1650, and 1573 cm^{-1} (associated with aliphatic or aromatic C═C or C═O structures),[54] near 1417 cm^{-1} (representing the bending vibration of aliphatic C−H bonds),[48] and 1030 cm^{-1} (related to the stretching vibration of C−O bonds).[49] These results suggest that the biochar possess multiple functional groups, which can potentially enhance the adsorption of NOR through $\pi-\pi$ interactions and hydrogen bonding.[55,56]

Figure 2b−d presents that the surfaces of KBC_{600}, KBC_{700}, and KBC_{800} are relatively rough. Increasing the pyrolysis

https://doi.org/10.1021/acsomega.4c03496
ACS Omega 2024, 9, 30813−30825

Table 2. Parameters for Adsorption Kinetics Fitting

parameters	NOR solution (mg/L)			
	25.00	50.00	100.0	150.0
		Pseudo-First-Order		
q_e (mg/g)	49.68	94.66	183.3	255.5
k_1 (min^{-1})	0.1785	0.1974	0.1824	0.1933
R^2	0.8719	0.8178	0.8174	0.7303
		Pseudo-Second-Order		
q_e (mg/g)	51.21	98.05	190.5	266.3
k_2 (min^{-1})	7.200×10^{-3}	4.210×10^{-3}	2.120×10^{-3}	1.080×10^{-3}
$t_{0.5}$ (min)	2.796	2.543	2.622	3.801
$t_{0.95}$ (min)	57.24	43.73	67.50	96.57
R^2	0.9638	0.9594	0.9559	0.9092
		Elovich		
α [mg/(g·min)]	3649	4457	4462	4788
β	0.2421	0.1233	0.06250	0.04230
R^2	0.7192	0.8085	0.8544	0.9216
		Intraparticle Diffusion		
$k_{d,1}$ (mg/(g·$min^{0.5}$))	8.850	17.37	33.16	43.49
C_1 (mg/g)	9.929	19.29	34.94	58.59
R^2	0.9695	0.9382	0.9723	0.9657
$k_{d,2}$ (mg/(g·$min^{0.5}$))	2.869	4.332	7.154	10.63
C_2 (mg/g)	31.09	61.08	123.7	163.7
R^2	0.9932	0.9854	0.9929	0.9913
$k_{d,3}$ (mg/(g·$min^{0.5}$))	0.01210	0.07210	0.5735	1.092
C_3 (mg/g)	50.34	96.70	180.4	247.0
R^2	0.7235	0.7855	0.7981	0.8336

temperature leads to more abundant pore structures on the surface of the materials owing to K_2CO_3 activation.[36,38] Among these samples, KBC_{800} exhibits a more porous structure (Figure S1c,d). Figure 2e,f demonstrates that the surface of KB and BC_{800} exhibits a relatively smooth lamellar structure without any obvious pore structure.

3.2. Effects of Adsorbent Dosage, Initial Concentration of NOR, Adsorption Time, and pH. The effectiveness of the adsorption process is contingent upon factors such as the quantity of adsorbent employed, the initial concentration of NOR, and the adsorption time. Increasing the amount of adsorbent initially improves the removal rate, but eventually stabilizes as the adsorption capacity decreases (Figure 3a). This is because more adsorbent provides more adsorption sites, allowing for faster removal of NOR. Once the adsorbent dosage reaches a sufficient level, complete adsorption of NOR in the solution occurs, leading to a gradual increase in the removal rates.[57] Specifically, a dosage increase from 0.2 to 1.0 g/L results in an increase in the removal rate from 38.43 to 99.95%. Further experiments were conducted with 0.5 g/L dosage to determine the adsorption capacity.

Higher initial concentration of the adsorbate typically enhances the adsorption capacity due to increased mass transfer driving forces.[58] Figure 3b shows that NOR adsorption capacity increases by KBC_{800} (from 47.29 to 567.9 mg/g) as its initial concentration increases from 25 to 400 mg/L. In spite of this, KBC_{800} has a limited number of active sites, resulting in a decreased removal efficiency.

As depicted in Figure 3c, the NOR removal rate is affected by the contact time. The NOR removal rate increases rapidly in the first hour, but further increasing the contact time does not significantly improve the removal efficiency. This may occur due to a reduced number of active sites on the KBC_{800} surface, leading to a decline in the concentration gradient of NOR between the solid and liquid phases. Consequently, the mass transfer driving force diminishes.[59]

As depicted in Figure 3d−f, within the pH range of 2−12, NOR adsorption capacity and removal efficiency initially increase and then decrease, caused by the zeta potential of KBC_{800} and the pK_a value of NOR. After adsorption, the pH_{pzc} of KBC_{800} + NOR increases, suggesting successful adsorption of NOR, particularly in the form of NOR^+ under acidic conditions.[6] As pH increases, electrostatic repulsion decreases, and the adsorption capacity of NOR increases. The highest removal efficiency of 90% is observed at pH 6, where there is electrostatic attraction between KBC_{800} and NOR within the pH range of 4−8.75. These findings suggest that the electrostatic interaction between NOR and KBC_{800} is a key factor in controlling the adsorption process.

3.3. Adsorption Kinetics. Various kinetic models were used to investigate the adsorption kinetics of NOR on KBC_{800}, including pseudo-first-order kinetics (PFO), pseudo-second-order kinetics (PSO), Elovich, and intraparticle diffusion (IPD) models (Figures 4a and S2). Table 2 presents the fitting parameters of these models for different initial NOR concentrations.

Initially, KBC_{800} adsorbs a lot of NOR molecules, thus increasing its adsorption capacity. As the reaction progresses, adsorption sites on KBC_{800} become fully occupied, leading to a decrease in adsorption rate. The PSO kinetic model shows higher R^2 values (0.9559−0.9638) than the PFO and Elovich models for NOR concentrations of 25−100 mg/L, indicating that it better describes the adsorption process at lower NOR concentrations. At a NOR concentration of 150 mg/L, the Elovich kinetic model has the highest R^2 value (0.9216), suggesting it aligns closely with the adsorption process, which is suitable for nonhomogeneous diffusion dominated by chemical adsorption.[38]

https://doi.org/10.1021/acsomega.4c03496
ACS Omega 2024, 9, 30813−30825

Table 3. Fitting Parameters for Adsorption Isotherms

	Langmuir model				Freundlich model			Sips model			
T (K)	$q_{e,exp}$ (mg/g)	q_m (mg/g)	K_L (L/mg)	R^2	K_F [(mg^{1-n} L^n)/g]	n	R^2	q_m (mg/g)	K_s (L/mg)^n	n	R^2
298	567.9	589.6	0.1897	0.9594	231.9	5.260	0.9038	589.4	0.1924	0.9024	0.9595
308	602.5	617.7	0.2557	0.9287	177.4	3.479	0.8620	617.7	0.2660	0.9162	0.9354
318	633.4	635.6	0.5028	0.9013	239.7	4.124	0.7738	634.1	0.5012	1.012	0.9037
328	666.2	659.7	0.6128	0.9292	265.2	4.045	0.7716	659.7	0.6182	1.097	0.9350

Table 4. Comparison of Maximum Adsorption Capacity of NOR by KBC_{800} with Selected Sorbents

adsorbent	carbonaceous precursor	surface area ($m^2 \cdot g^{-1}$)	adsorption capacity ($mg \cdot g^{-1}$)	adsorption conditions	references
KBC_{800}	*Atropa belladonna* L	1638	666.2	C_0 = 25−400 mg L^{-1}, 308 K, 0.5 g L^{-1} of KBC_{800}	this study
NH_3-MBC	corn stalk feedstock	209.0	12.00	C_0 = 5−50 mg L^{-1}, 298 K, 1 g L^{-1} of NH_3-MBC	31
BC	luffa sponge	822.0	286.0	C_0 = 50−200 mg L^{-1}, 288 K, 0.5 g L^{-1} of BC	32
N-A-CSB700	cocoa shells	328.0	133.0	C_0 = 10−300 mg L^{-1}, 298 K, 1 g L^{-1} of N-A-CSB700	11
AIS-KLB	biochar	44.00	42.00	C_0 = 1−20 mg L^{-1}, 298 K, 0.5 g L^{-1} of AIS-KLB	27
APB	potato stems	90.00	5.000	C_0 = 5−50 mg L^{-1}, 308 K, 10 g L^{-1} of APB	29
SCGB	spent coffee grounds	46.00	70.00	C_0 = 10−50 mg L^{-1}, 298 K, 1 g L^{-1} of SCGB	25
HLB	corn straw	1537	519.0	C_0 = 0−400 mg L^{-1}, 318 K, 0.4 g L^{-1} of HLB	38

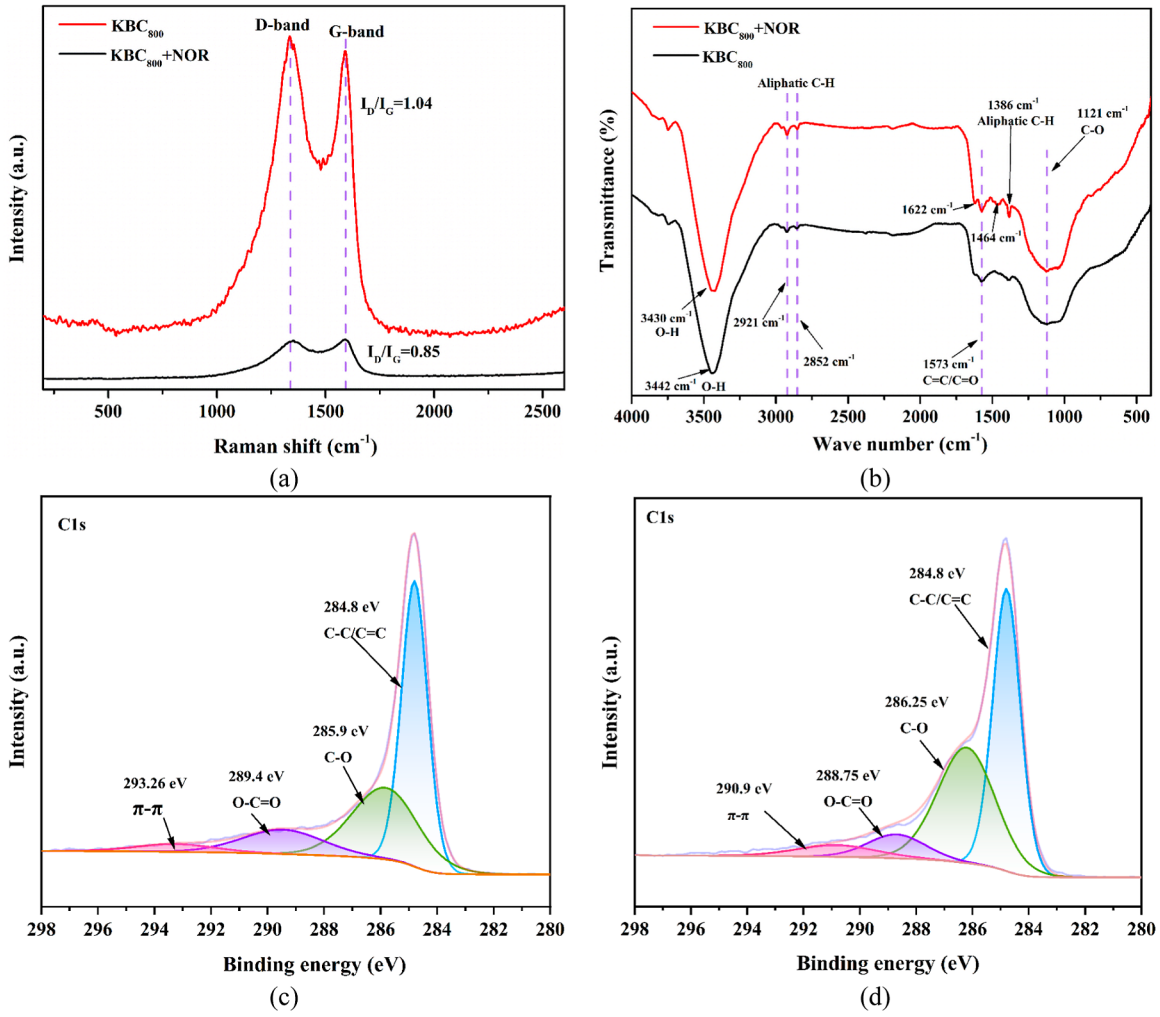

Figure 5. Raman spectra (a) and FTIR (b) of KBC_{800} and KBC_{800} + NOR; XPS spectra of C 1s for KBC_{800} (c) and KBC_{800} + NOR (d).

In order to determine the time required for the system to attain, the terms $t_{0.5}$ and $t_{0.95}$ are employed to denote the time necessary for the adsorption to reach 50 and 95% saturation, respectively.[59,60] According to the PSO model, the calculated values of $t_{0.5}$ and $t_{0.95}$ indicate that the adsorption capacity has reached 50% of the saturated adsorption capacity within 4 min and 95% of the equilibrium adsorption capacity within the range of 57−97 min, completing the efficient removal of NOR.

https://doi.org/10.1021/acsomega.4c03496
ACS Omega 2024, 9, 30813−30825

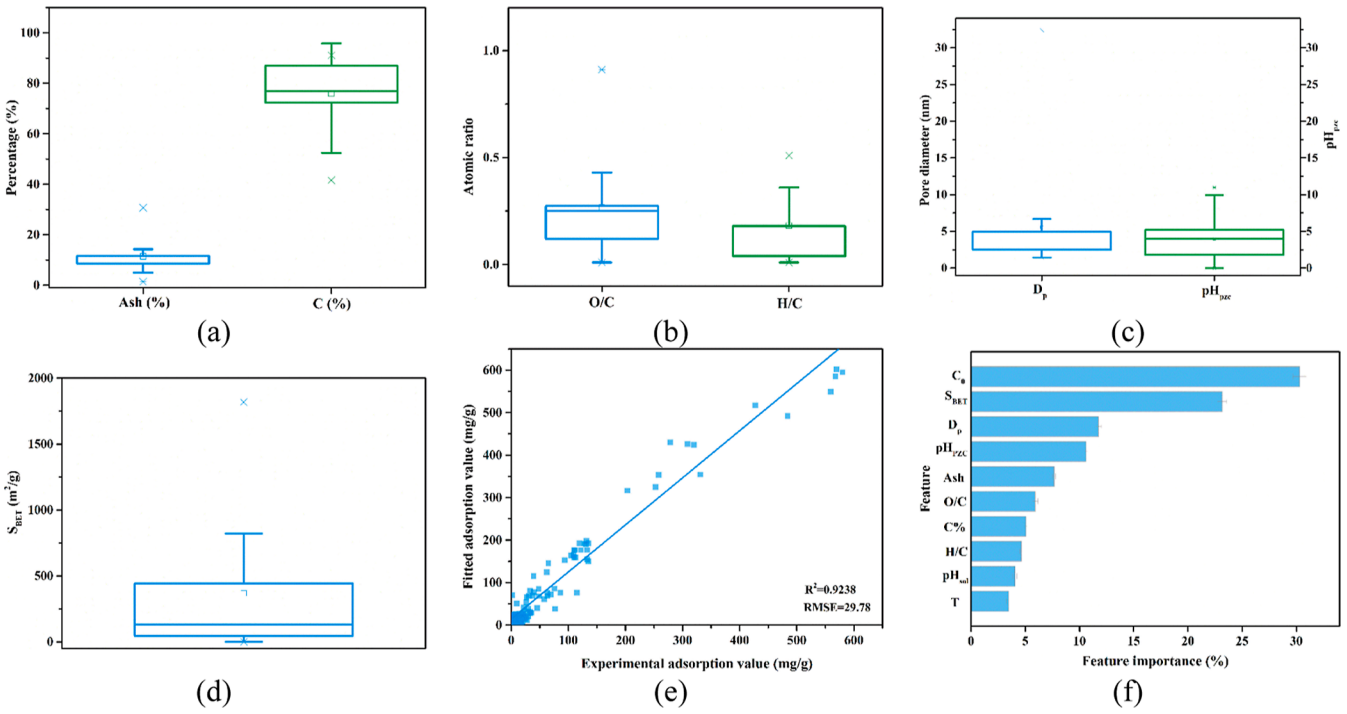

Figure 6. Boxplot of BC physicochemical properties (a−d); comparison between the fitting of data by the RF model and the experimental data (e); relative importance of input variables on adsorption efficiency (f).

The slopes of the three lines in the IPD model decrease as adsorption continues, with $k_{d,1}$ having the highest value and $k_{d,3}$ the lowest (Figure S2c and Table 2). Initially, NOR diffuses quickly to the KBC_{800} surface. As the reaction proceeds, the NOR concentration decreases, resulting in a decrease in mass transfer driving force. Diffusion resistance increases during the second stage as NOR molecules enter the pores, causing a decrease in adsorption rates. The third stage shows the smallest slope, signifying equilibrium in the reaction. The absence of fitting lines passing through the origin suggests that IPD is not the sole rate-controlling step of adsorption, both IPD and surface adsorption play a role in regulating the adsorption rate.[38,61]

3.4. Adsorption Isotherms and Thermodynamic. The Langmuir, Freundlich, and Sips models were employed to fit the adsorption isotherm (Figures 4b and S3 and Table 3). The R^2 value of the Sips model is the highest for the sample KBC_{800}, indicating a complex adsorption mechanism for NOR involving both monolayer and multilayer adsorption processes, rather than ideal monolayer adsorption. Additionally, it can be observed that the maximum experimental adsorption capacity of NOR on KBC_{800} is about 666.2 mg/g, which is higher than most of the reported carbon-based adsorbents (Table 4). Based on the Van't Hoof equation, a series of thermodynamic parameters were calculated.[62−66] The thermodynamic analysis in Figure S4 and Table S5 shows that as temperature rises from 298 to 328 K, ΔG decreases and becomes negative, suggesting that NOR adsorption by KBC_{800} is spontaneous and favored at higher temperatures. The ΔH of KBC_{800} is 32.49 kJ/mol, suggesting an endothermic process with physical interactions. The positive ΔS presents an increase in randomness at the solid−liquid interface during adsorption, promoting the adsorption progress.[41]

3.5. Effects of Competitive Ions/Antibiotics. Competitive ions like CO_3^{2-}, HCO_3^-, SO_4^{2-}, Na^+, K^+, Ca^{2+}, and Mg^{2+} were studied in wastewater for their impact on NOR removal. At 1 mmol/L, the NOR removal rate was 99.8%, but decreased at 100 mmol/L, indicating competition for adsorption sites (Figure 4c).[67] Overall, the presence of competitive ions has minimal influence on NOR adsorption, signifying that the KBC_{800} biochar is a highly promising adsorbent for NOR and is resistant to interference from impurity ions.

Furthermore, alongside common ions, diverse antibiotics, including ERY, PEN-G, OTC, and SUL, are also present in wastewater. At 10 mg/L, KBC_{800} removes over 98.6% of NOR, but at higher concentrations of ERY, OTC, and SUL, the removal rates decrease to 94.5, 91.57, and 81.09%, respectively, indicating competition between NOR and other antibiotics (Figure 4d). In particular, we used ultraviolet dual-wavelength spectrophotometry for the measurement of NOR in OTC and SUL systems (Figure S5). This competitive adsorption is owing to the abundance of π electrons, aromatic structures, and oxygen-containing functional groups in these three antibiotics, which can form $\pi-\pi$ interactions and hydrogen bonds with KBC_{800}. SUL, which has a structure most similar to norfloxacin, shows the strongest competitive adsorption.[68]

3.6. Adsorption Mechanism. It was found that S_{BET} decreased from 1638 to 271 m^2/g, and the V_{total} decreased from 1.07 to 0.232 cm^3/g after NOR adsorption (Figure S6 and Table S6), indicating pore occupation. NOR molecules (1.36 nm × 1.0 nm × 0.64 nm)[38] with a size smaller than the average pore size of KBC_{800} entered the pores. KBC_{800} showed an increase in pore size after adsorption, confirming that pores were occupied, and the pore filling was critical to NOR adsorption.

In Figure 5a of the Raman spectra, two peaks, the D peak and G peak, were observed at approximately 1335 and 1590 cm^{-1}, respectively. The I_D/I_G ratio decreased significantly from 1.04 to 0.85 after NOR adsorption on KBC_{800}, indicating strong $\pi-\pi$ interactions.[38] The shift in the −OH absorption peak from 3442 to 3430 cm^{-1} in the infrared spectra in Figure 5b suggests the

https://doi.org/10.1021/acsomega.4c03496
ACS Omega 2024, 9, 30813−30825

presence of hydrogen bonds between NOR and oxygen-containing functional groups on the surface of KBC_{800} after NOR adsorption.[38] Furthermore, new peaks at 1622 and 1464 cm^{-1} in KBC_{800} + NOR suggest successful adsorption of NOR onto KBC_{800}. The benzene ring in NOR acts as an electron acceptor, interacting with the hydroxyl group and benzene ring on the adsorbent through $\pi-\pi$ interactions, leading to a decrease in I_D/I_G.

Figure S7 shows N and F absorption peaks in the XPS spectra after adsorption, suggesting successful adsorption of NOR by KBC_{800}. The C 1s spectrum (Figure 5c,d) presents a shift in peak from 285.9 to 286.25 eV, suggesting electron-donating properties of the C−O bond on the adsorbent. The shift in the peak from 289.1 to 288.75 eV indicates electron-accepting properties of O−C−O moiety.[69] The O 1s spectrum (Figure S7) shows a shift in peak from 533.78 to 533.34 eV, suggesting that the C═O functional group can act as an electron acceptor.[48,54] These oxygen-containing functional groups can engage in a π-electron donor−acceptor interaction with NOR molecules, thereby facilitating the adsorption of NOR.

3.7. Regeneration Ability. According to Figure S8, the investigation of the stability and regeneration capability of KBC_{800} was conducted through a six-cycle adsorption experiment. Even after six adsorption cycles, the removal rate of NOR remains at 82%, and the desorption rate was also as high as 77%. This indicates that KBC_{800} has good regeneration capability, making it a promising adsorbent for the treatment of antibiotic-containing wastewater.

3.8. Prediction of NOR Adsorption Based on the ML Model. This study analyzed 44 carbon materials using box plots (Figure 6). The chosen BC materials contain 52.3−95.4% C and have an average ash content of 11.8%. The average O/C ratio is 0.25, and the average H/C ratio is 0.19. The S_{BET} ranges from 8.72 to 818 m^2/g. NOR adsorption is greatly affected by the average pore size of BC (1.53 to 6.65 nm). Meanwhile, a wide range of pH_{pzc} values (0.13−9.8) can be observed in Figure 6c, indicating that most BC surfaces in neutral or alkaline solutions carry a negative charge.

Figure S9 shows the Pearson correlation matrix for BC properties. Strong relationships are indicated by high correlation coefficients. Negative correlation between C % and O/C (−0.957) and positive correlations with S_{BET} are observed. Additionally, strong positive correlations (0.945 and 0.808) are also seen with q_e, C_0, and S_{BET}. By controlling BC properties and application conditions, adsorption capacity can be increased.

An RF algorithm was employed to develop a model for NOR adsorption on BC. The model's performance was evaluated using 30% of the test data and compared to experimental results (Figure 6e and Table S7). The R^2 value of the model is 0.9238, indicating a strong fit between BC and NOR adsorption. This suggests that the model is reliable in predicting adsorption across different conditions and properties of BC. The cross-validation results reveal minimal disparity in the distribution range and average values of R^2 and RMSE between the training and testing sets, indicating consistent performance of the model. Furthermore, the model displays comparable efficacy on both sets and shows strong generalization capabilities (Figure S10).

Studying how BC's properties affect its adsorption performance is crucial for designing effective BC. This study used the RMSE loss function to assess variable importance. Results in Figure 6f indicate that NOR adsorption capacity is primarily influenced by C_0. Increasing the concentration gradient between the aqueous phase and the adsorbent surface promotes NOR adsorption on BC. A higher S_{BET} offers more active sites for NOR adsorption, and the average pore size of BC also affects NOR adsorption capacity. There is also a significant effect of pH_{pzc} on the adsorption capacity, followed by ash (7.7%), O/C (6.0%), C content (5.0%), and H/C (4.7%). These factors are ranked in order of their influence on NOR adsorption capacity in aqueous solutions.

3.9. Dependence of BC Properties and Adsorption Conditions on NOR Adsorption Performance. RF analysis identified C_0, S_{BET}, D_P, and pH_{pzc} as key factors for NOR adsorption on BC. Figure S10 illustrates the correlation between these factors and NOR adsorption efficiency, with high NOR to adsorbent ratio leading to increased adsorption. S_{BET} has a significant impact on NOR adsorption, particularly between 0 and 1800 m^2/g, while pore size also plays a crucial role (Figure S11b,c). Excessively large pore sizes do not help with NOR adsorption. Additionally, the pH_{pzc} value of BC also affects NOR adsorption, with a nonlinear impact on adsorption capacity (Figure S11d). The pH_{pzc} value determines the surface charge of BC at different pH_{sol}. NOR species include NOR^+, NOR^0, and NOR^-, depending on pH levels. NOR adsorption dependence on pH_{pzc} increases from 0 to 4 and stays the same from 4.5 to 6, likely due to electrostatic interaction.

4. CONCLUSIONS

In this study, the utilization of biomass waste derived from CHM residues as a raw material for the production of biochar was investigated. The produced biochar, characterized by a substantial BET surface area of 1638 $m^2\ g^{-1}$ and an abundance of functional surface groups, was employed for the removal of NOR from wastewater. The adsorption process of NOR on KBC_{800} was found to be well-described by the Sips isotherm model. Through experimentation, it was determined that the maximum adsorption capacity of NOR on KBC_{800} was 666.2 mg/g at 328 K. The thermodynamic analysis revealed that the interaction between NOR and KBC_{800} in the adsorption system was both spontaneous and exothermic. Moreover, KBC_{800} removes NOR primarily by the pore filling, with electrostatic attraction, $\pi-\pi$ interactions, and hydrogen bonding also contributing to its effectiveness. Even after undergoing six cycles of adsorption−desorption, KBC_{800} still exhibited an impressive 82% removal rate of NOR. ML analysis revealed that the initial concentration had the greatest influence on NOR adsorption by the BC, followed by S_{BET} and average pore size. The assessment of relative importance and partial dependence plots can provide effective guidance for rational utilization of carbon materials in the treatment of NOR-containing wastewater.

■ ASSOCIATED CONTENT

Supporting Information

The Supporting Information is available free of charge at https://pubs.acs.org/doi/10.1021/acsomega.4c03496.

Characterization method; ML methods; pore size distribution and SEM of ABL biochar; adsorption kinetics fitting; adsorption isotherm fitting; adsorption thermodynamic fitting; UV full-wavelength spectrum; N_2 adsorption−desorption isotherm of KBC_{800} + NOR; XPS; circulation regeneration experiment; pearson correlation matrix; comparison of RMSE and R^2 between the training and testing set; partial dependence plot; adsorption equation; data collection of ML; examples of group

https://doi.org/10.1021/acsomega.4c03496
ACS Omega 2024, 9, 30813−30825

labeling for the selected materials in the ML process; elemental content of ABL biochar; thermodynamic calculation parameters; parameters of pore structures for KBC_{800} + NOR and evaluation of the test set and training set allocation ratio (PDF)

AUTHOR INFORMATION

Corresponding Author

Zhijuan Zhang − *College of Pharmacy, Henan University of Chinese Medicine, Zhengzhou 450046, China; Institute of Mass Spectrometer and Atmospheric Environment, Jinan University, Guangzhou 510632, China;* orcid.org/0000-0002-9451-2394; Email: zhangyan0204@126.com

Authors

Miaomiao Zhang − *College of Pharmacy, Henan University of Chinese Medicine, Zhengzhou 450046, China*

Pengwei Li − *College of Pharmacy, Henan University of Chinese Medicine, Zhengzhou 450046, China*

Dong Guo − *College of Pharmacy, Henan University of Chinese Medicine, Zhengzhou 450046, China*

Ziheng Zhao − *College of Pharmacy, Henan University of Chinese Medicine, Zhengzhou 450046, China*

Weisheng Feng − *College of Pharmacy, Henan University of Chinese Medicine, Zhengzhou 450046, China*

Complete contact information is available at: https://pubs.acs.org/10.1021/acsomega.4c03496

Author Contributions

[§]M.Z. and P.L. contributed equally. **Miaomiao Zhang**: Conceptualization, methodology, data curation, visualization, formal analysis, and writing—original draft. **Pengwei Li**: Conceptualization, methodology, visualization, and writing—review and editing. **Dong Guo**: Conceptualization, methodology, and visualization. **Ziheng Zhao**: Conceptualization and methodology. **Weisheng Feng**: Methodology and supervision. **Zhijuan Zhang**: Conceptualization, methodology, supervision, funding acquisition, and writing—review and editing.

Notes

The authors declare no competing financial interest.

ACKNOWLEDGMENTS

The authors thank the Natural Science Foundation of Henan (grant 242300420197), National Natural Science Foundation of China (grant 21878122), and Zhongjing Core Scholar's Research Initial Fund of Henan University of Chinese Medicine for financial support.

REFERENCES

(1) Kovalakova, P.; Cizmas, L.; McDonald, T. J.; Marsalek, B.; Feng, M.; Sharma, V. K. Occurrence and toxicity of antibiotics in the aquatic environment: A review. *Chemosphere* **2020**, *251*, 126351.

(2) Elder, F. C. T.; Feil, E. J.; Snape, J.; Gaze, W. H.; Kasprzyk-Hordern, B. The role of stereochemistry of antibiotic agents in the development of antibiotic resistance in the environment. *Environ. Int.* **2020**, *139*, 105681.

(3) Kumar, A.; Pal, D. Antibiotic resistance and wastewater: Correlation, impact and critical human health challenges. *J. Environ. Chem. Eng.* **2018**, *6* (1), 52−58.

(4) Brienza, M.; Sauvêtre, A.; Ait-Mouheb, N.; Bru-Adan, V.; Coviello, D.; Lequette, K.; Patureau, D.; Chiron, S.; Wéry, N. Reclaimed wastewater reuse in irrigation: Role of biofilms in the fate of antibiotics and spread of antimicrobial resistance. *Water Res.* **2022**, *221*, 118830.

(5) Huang, L.; Mo, Y.; Wu, Z.; Rad, S.; Song, X.; Zeng, H.; Bashir, S.; Kang, B.; Chen, Z. Occurrence, distribution, and health risk assessment of quinolone antibiotics in water, sediment, and fish species of Qingshitan reservoir, South China. *Sci. Rep.* **2020**, *10* (1), 15777.

(6) Luo, J.; Li, X.; Ge, C.; Müller, K.; Yu, H.; Deng, H.; Shaheen, S. M.; Tsang, D. C. W.; Bolan, N. S.; Rinklebe, J.; et al. Preparation of ammonium-modified cassava waste-derived biochar and its evaluation for synergistic adsorption of ternary antibiotics from aqueous solution. *J. Environ. Manage.* **2021**, *298*, 113530.

(7) Li, X.; Jiang, H.; Zhu, L.; Tang, J.; Liu, Z.; Dai, Y. Adsorption interactions between typical microplastics and enrofloxacin: Relevant contributions to the mechanism. *Chemosphere* **2024**, *351*, 141181.

(8) Ricky, R.; Shanthakumar, S. A pilot-scale study on the removal of binary mixture (ciprofloxacin and norfloxacin) by Scenedesmus obliquus: Optimization, biotransformation, and biofuel profile. *J. Environ. Manage.* **2023**, *344*, 118388.

(9) Wang, P.; Zhang, H.; Wu, Z.; Zhao, X.; Sun, Y.; Duan, N.; Liu, Z.; Liu, W. A data-based review on norfloxacin degradation by persulfate-based advanced oxidation processes: Systematic evaluation and mechanisms. *Chin. Chem. Lett.* **2023**, *34* (12), 108722.

(10) Chen, B.; Wang, J.; Li, R.; Lin, H.; Li, B.; Shen, L.; Xu, Y.; Zhang, M. Fabrication of $CoFe_2O_4/Mn_3O_4$ decorated ultrathin graphitic carbon nitride nanosheets membrane for persistent organic pollutants removal: Synergistic performance and mechanisms. *Sep. Purif. Technol.* **2023**, *309*, 123076.

(11) Guy Laurent Zanli, B. L.; Tang, W.; Chen, J. N-doped and activated porous biochar derived from cocoa shell for removing norfloxacin from aqueous solution: Performance assessment and mechanism insight. *Environ. Res.* **2022**, *214*, 113951.

(12) Jiang, H.; Dai, Y. Vitamin C modified crayfish shells biochar efficiently remove tetracycline from water: A good medicine for water restoration. *Chemosphere* **2023**, *311*, 136884.

(13) Bouaziz, N.; Kouira, O.; Aouaini, F.; Bukhari, L.; Knani, S.; Znaidia, S.; Lamine, A. B. Adsorption of antibiotics by bentonite-chitosan composite: Phenomenological modeling and physical investigation of the adsorption process. *Int. J. Biol. Macromol.* **2023**, *242*, 125156.

(14) Geng, R.; Wang, J.; Zhang, Z.; Dong, Q.; Wu, F.; Chen, S.; Su, T.; Qi, X. Adsorption of antibiotics by polydopamine-modified salecan hydrogel: Performance, kinetics and mechanism studies. *Chem. Eng. J.* **2023**, *454*, 140446.

(15) Han, L.; Qin, P.; Li, M.; Li, D.; Mu, M.; Gao, Y.; Zhu, S.; Lu, M.; Cai, Z. Hierarchically porous zirconium-based metal-organic frameworks for rapid adsorption and enrichment of sulfonamide antibiotics. *Chem. Eng. J.* **2023**, *456*, 140969.

(16) Jiang, H.; Li, X.; Dai, Y. Phosphoric acid activation of cow dung biochar for adsorbing enrofloxacin in water: Icing on the cake. *Environ. Pollut.* **2024**, *341*, 122887.

(17) Wang, Z.; Wang, G.; Li, W.; Cui, Z.; Wu, J.; Akpinar, I.; Yu, L.; He, G.; Hu, J. Loofah activated carbon with hierarchical structures for high-efficiency adsorption of multi-level antibiotic pollutants. *Appl. Surf. Sci. Adv.* **2021**, *550*, 149313.

(18) Srivastava, G. P.; Chadha, T. N. Effect of surface-active agents on the extraction of belladonna herb. *J. Pharm. Sci.* **1963**, *52* (3), 299−301.

(19) Li, P.; Zhao, T.; Zhao, Z.; Tang, H.; Feng, W.; Zhang, Z. Biochar derived from Chinese herb medicine residues for rhodamine B dye adsorption. *ACS Omega* **2023**, *8* (5), 4813−4825.

(20) Liu, Z.; Zhang, J.; Zhang, L.; Guan, Y.; Ji, H.; Zhang, Y.; Gao, H. Efficient removal of Congo red and methylene blue using biochar from Medulla Tetrapanacis modified by potassium carbonate. *Bioresour. Technol.* **2023**, *376*, 128912.

(21) Sayğılı, H.; Sayğılı, G. A. Optimized preparation for bimodal porous carbon from lentil processing waste by microwave-assisted K_2CO_3 activation: Spectroscopic characterization and dye decolorization activity. *J. Clean Prod.* **2019**, *226*, 968−976.

(22) Maulana Kusdhany, M. I.; Lyth, S. M. New insights into hydrogen uptake on porous carbon materials via explainable machine learning. *Carbon* **2021**, *179*, 190−201.

(23) Zhang, K.; Zhong, S.; Zhang, H. Predicting aqueous adsorption of organic compounds onto biochars, carbon nanotubes, granular activated carbons, and resins with machine learning. *Environ. Sci. Technol.* **2020**, *54* (11), 7008−7018.
(24) Wang, J.; Zhang, M.; Zhou, R.; Li, J.; Zhao, W.; Zhou, J. Adsorption characteristics and mechanism of norfloxacin in water by γ-Fe_2O_3@BC. *Water Sci. Technol.* **2020**, *78* (2020), 124562.
(25) Nguyen, V.-T.; Vo, T.-D.-H.; Nguyen, T.-B.; Dat, N. D.; Huu, B. T.; Nguyen, X.-C.; Tran, T.; Le, T.-N.-C.; Duong, T.-G.-H.; Bui, M.-H.; et al. Adsorption of norfloxacin from aqueous solution on biochar derived from spent coffee ground: Master variables and response surface method optimized adsorption process. *Chemosphere* **2022**, *288*, 132577.
(26) Zhang, J.; Lu, M.; Wan, J.; Sun, Y.; Lan, H.; Deng, X. Effects of pH, dissolved humic acid and Cu^{2+} on the adsorption of norfloxacin on montmorillonite-biochar composite derived from wheat straw. *Biochem. Eng. J.* **2018**, *130*, 104−112.
(27) Yang, Y.; Zhong, Z.; Li, J.; Du, H.; Li, Z. Efficient with low-cost removal and adsorption mechanisms of norfloxacin, ciprofloxacin and ofloxacin on modified thermal kaolin: experimental and theoretical studies. *J. Hazard. Mater.* **2022**, *430*, 128500.
(28) Cheng, L.; Ji, Y.; Shao, Q. Facile modification of hydrochar derived from cotton straw with excellent sorption performance for antibiotics: Coupling DFT simulations with experiments. *Sci. Total Environ.* **2021**, *760*, 144124.
(29) Jing, F.; Guan, J.; Tang, W.; Chen, J. Mechanistic insight into adsorptive removal of ionic NOR and nonionic DEP organic contaminates by clay-biochar composites. *Environ. Pollut.* **2022**, *310*, 119881.
(30) He, S.; Chen, Q.; Chen, G.; Shi, G.; Ruan, C.; Feng, M.; Ma, Y.; Jin, X.; Liu, X.; Du, C.; et al. N-doped activated carbon for high-efficiency ofloxacin adsorption. *Microporous Mesoporous Mater.* **2022**, *335*, 111848.
(31) Wu, J.; Wang, T.; Liu, Y.; Tang, W.; Geng, S.; Chen, J. Norfloxacin adsorption and subsequent degradation on ball-milling tailored N-doped biochar. *Chemosphere* **2022**, *303*, 135264.
(32) Feng, Y.; Liu, Q.; Yu, Y.; Kong, Q.; Zhou, L.-l.; Du, Y.-d.; Wang, X.-f. Norfloxacin removal from aqueous solution using biochar derived from luffa sponge. *J. Water Supply Res. Technol. -Aqua* **2018**, *67* (8), 703−714.
(33) Li, Y.; Zhu, J.; Xie, C.; Xie, X.; Wang, Z.; Qin, T. A novel biochar derived from cauliflower (Brassica oleracea L.) roots could remove norfloxacin and chlortetracycline efficiently. *Water Sci. Technol.* **2017**, *76* (12), 3307−3318.
(34) Li, Y.; Wang, Z.; Xie, X.; Zhu, J.; Li, R.; Qin, T. Removal of norfloxacin from aqueous solution by clay-biochar composite prepared from potato stem and natural attapulgite. *Colloids Surf., A* **2017**, *514*, 126−136.
(35) Paredes-Laverde, M.; Silva-Agredo, J.; Torres-Palma, R. A. Removal of norfloxacin in deionized, municipal water and urine using rice (Oryza sativa) and coffee (Coffea arabica) husk wastes as natural adsorbents. *J. Environ. Manage.* **2018**, *213*, 98−108.
(36) Luo, J.; Li, X.; Ge, C.; Müller, K.; Yu, H.; Huang, P.; Li, J.; Tsang, D. C. W.; Bolan, N. S.; Rinklebe, J.; et al. Sorption of norfloxacin, sulfamerazine and oxytetracycline by KOH-modified biochar under single and ternary systems. *Bioresour. Technol.* **2018**, *263*, 385−392.
(37) Zhu, L.; Zhao, N.; Tong, L.; Lv, Y. Structural and adsorption characteristics of potassium carbonate activated biochar. *RSC Adv.* **2018**, *8* (37), 21012−21019.
(38) Zhou, H.; Wang, Z.; Gao, C.; Sun, Q.; Liu, J.; She, D. Synthesis of honeycomb lignin-based biochar and its high-efficiency adsorption of norfloxacin. *Bioresour. Technol.* **2023**, *369*, 128402.
(39) Shen, Y.; Zhang, N.; Zhang, S. Catalytic pyrolysis of biomass with potassium compounds for Co-production of high-quality biofuels and porous carbons. *Energy* **2020**, *190*, 116431.
(40) Liu, Z.; Wei, Y.; Alsohaimi, I. H. K_2CO_3-activated pomelo peels as a high-performance adsorbent for removal of Cu(II): preparation, characterization, and adsorption studies. *J. Chem.* **2021**, *2021*, 1−11.
(41) Zhang, Z.; Sun, L.; Pei, Z.; Li, H.; Wang, L.; Ma, J.; Li, Y.; Yang, R.; Zhang, Q. New insight into the adsorption of sulfadiazine on graphite-like biochars prepared at different pyrolytic temperatures. *J. Clean Prod.* **2023**, *413*, 137468.
(42) Wang, Q.; Fagbohun, E. O.; Zhu, H.; Hussain, A.; Wang, F.; Cui, Y. One-step synthesis of magnetic asphalt-based activated carbon with high specific surface area and adsorption performance for methylene blue. *Sep. Purif. Technol.* **2023**, *321*, 124205.
(43) Taheri, E.; Fatehizadeh, A.; Lima, E. C.; Rezakazemi, M. High surface area acid-treated biochar from pomegranate husk for 2,4-dichlorophenol adsorption from aqueous solution. *Chemosphere* **2022**, *295*, 133850.
(44) Guo, X.; Zhu, L.; Xu, X.; Ma, M.; Zou, G.; Wei, D. Competitive or synergetic? Adsorption mechanism of phosphate and oxytetracycline on chestnut shell-derived biochar. *J. Clean Prod.* **2022**, *370*, 133526.
(45) Yang, X.; Wang, L.; Tong, J.; Shao, X.; Chen, R.; Yang, Q.; Li, F.; Xue, B.; Li, G.; Han, Y.; et al. Synthesis of hickory biochar via one-step acidic ball milling: Characteristics and titan yellow adsorption. *J. Clean Prod.* **2022**, *338*, 130575.
(46) Xu, L.; Wu, C.; Chai, C.; Cao, S.; Bai, X.; Ma, K.; Jin, X.; Shi, X.; Jin, P. Adsorption of micropollutants from wastewater using iron and nitrogen co-doped biochar: Performance, kinetics and mechanism studies. *J. Hazard. Mater.* **2022**, *424* (2022), 127606.
(47) Zhang, Y.; Zheng, Y.; Yang, Y.; Huang, J.; Zimmerman, A. R.; Chen, H.; Hu, X.; Gao, B. Mechanisms and adsorption capacities of hydrogen peroxide modified ball milled biochar for the removal of methylene blue from aqueous solutions. *Bioresour. Technol.* **2021**, *337*, 125432.
(48) Appiah-Ntiamoah, R.; Tilahun, K. M.; Mengesha, D. N.; Weldesemat, N. T.; Ruello, J. L.; Egualle, F. K.; Ganje, P.; Kim, H. Carbonyl-interfaced-biochar derived from unique capillary structures via one-step carbonization with selective methyl blue adsorption capability. *J. Clean Prod.* **2023**, *410*, 137291.
(49) Liu, L.; Li, X.; Wang, X.; Wang, Y.; Shao, Z.; Liu, X.; Shan, D.; Liu, Z.; Dai, Y. Metolachlor adsorption using walnut shell biochar modified by soil minerals. *Environ. Pollut.* **2022**, *308*, 119610.
(50) Zhang, Y.; Zhang, J.; Chen, K.; Shen, S.; Hu, H.; Chang, M.; Chen, D.; Wu, Y.; Yuan, H.; Wang, Y. Engineering banana-peel-derived biochar for the rapid adsorption of tetracycline based on double chemical activation. *Resour. Conserv. Recycl.* **2023**, *190* (2023), 106821.
(51) Oginni, O.; Singh, K. Effect of carbonization temperature on fuel and caffeine adsorption characteristics of white pine and Norway spruce needle derived biochars. *Ind. Crop. Prod.* **2021**, *162* (2021), 113261.
(52) Chen, X.; Guo, Z.; Liu, J.; Wu, F.; Cheng, C.; Lin, H.; Ren, W.; Zhang, H. Electron transfer-based peroxydisulfate activation by waste herb residue biochar: Adsorption versus surface oxidation. *Chem. Eng. J.* **2023**, *451* (2023), 138560.
(53) Nguyen, T.-B.; Nguyen, T.-K.-T.; Chen, W.-H.; Chen, C.-W.; Bui, X.-T.; Patel, A. K.; Dong, C.-D. Hydrothermal and pyrolytic conversion of sunflower seed husk into novel porous biochar for efficient adsorption of tetracycline. *Bioresour. Technol.* **2023**, *373*, 128711.
(54) Huang, K.; Yang, S.; Liu, X.; Zhu, C.; Qi, F.; Wang, K.; Wang, J.; Wang, Q.; Wang, T.; Ma, P. Adsorption of antibiotics from wastewater by cabbage-based N, P co-doped mesoporous carbon materials. *J. Clean Prod.* **2023**, *391*, 136174.
(55) Yao, B.; Luo, Z.; Du, S.; Yang, J.; Zhi, D.; Zhou, Y. Sustainable biochar/$MgFe_2O_4$ adsorbent for levofloxacin removal: Adsorption performances and mechanisms. *Bioresour. Technol.* **2021**, *340* (2021), 125698.
(56) Liu, Y.; Yuan, Y.; Wang, Z.; Wen, Y.; Liu, L.; Wang, T.; Xie, X. Removal of ofloxacin from water by natural ilmenite-biochar composite: A study on the synergistic adsorption mechanism of multiple effects. *Bioresour. Technol.* **2022**, *363* (2022), 127938.
(57) Daware, G. B.; Gogate, P. R. Removal of pyridine using ultrasound assisted and conventional batch adsorption based on tea waste residue as biosorbent. *Environ. Technol. Innov.* **2021**, *21* (2021), 101292.

https://doi.org/10.1021/acsomega.4c03496
ACS Omega 2024, 9, 30813−30825

(58) Cavalcante, E. H. M.; Candido, I. C. M.; de Oliveira, H. P.; Silveira, K. B.; Víctor de Souza Álvares, T.; Lima, E. C.; Thyrel, M.; Larsson, S. H.; Simões dos Reis, G. 3-aminopropyl-triethoxysilane-functionalized tannin-rich grape biomass for the adsorption of methyl orange dye: Synthesis, characterization, and the adsorption mechanism. *ACS Omega* **2022**, *7* (22), 18997−19009.
(59) Dos Reis, G. S.; Bergna, D.; Grimm, A.; Lima, E. C.; Hu, T.; Naushad, M.; Lassi, U. Preparation of highly porous nitrogen-doped biochar derived from birch tree wastes with superior dye removal performance. *Colloids Surf., A* **2023**, *669*, 131493.
(60) Dos Reis, G. S.; Thivet, J.; Laisné, E.; Srivastava, V.; Grimm, A.; Lima, E. C.; Bergna, D.; Hu, T.; Naushad, M.; Lassi, U. Synthesis of novel mesoporous selenium-doped biochar with high-performance sodium diclofenac and reactive orange 16 dye removals. *Chem. Eng. Sci.* **2023**, *281*, 119129.
(61) Yang, Y.; Cannon, F. S. Biomass activated carbon derived from pine sawdust with steam bursting pretreatment; perfluorooctanoic acid and methylene blue adsorption. *Bioresour. Technol.* **2022**, *344*, 126161.
(62) Liu, Y.; Xu, H. Equilibrium, thermodynamics and mechanisms of Ni^{2+} biosorption by aerobic granules. *Biochem. Eng. J.* **2007**, *35* (2), 174−182.
(63) Lima, E. C.; Hosseini-Bandegharaei, A.; Moreno-Piraján, J. C.; Anastopoulos, I. A critical review of the estimation of the thermodynamic parameters on adsorption equilibria. Wrong use of equilibrium constant in the Van't Hoof equation for calculation of thermodynamic parameters of adsorption. *J. Mol. Liq.* **2019**, *273*, 425−434.
(64) Liu, Y.; Liu, Y.-J. Biosorption isotherms, kinetics and thermodynamics. *Sep. Purif. Technol.* **2008**, *61* (3), 229−242.
(65) Wu, J.; Yang, J.; Huang, G.; Xu, C.; Lin, B. Hydrothermal carbonization synthesis of cassava slag biochar with excellent adsorption performance for Rhodamine B. *J. Clean Prod.* **2020**, *251*, 119717.
(66) Liu, Y. Is the free energy change of adsorption correctly calculated? *J. Chem. Eng. Data* **2009**, *54*, 1981−1985.
(67) Sun, Y.; Liu, C.; Gao, Y.; Zhang, T.; Jia, Y.; Wang, S. All-in-one strategy to prepare molded biochar with magnetism from sewage sludge for high-efficiency removal of Cd(II). *J. Hazard. Mater.* **2023**, *454*, 131488.
(68) Bi, Z.; Li, T.; Xing, X.; Qi, P.; Li, Z.; Hu, C.; Xu, X.; Sun, Z.; Xu, G.; Chen, C.; et al. Contribution of extracellular polymeric substances and microbial community on the safety of drinking water quality: By mean of Cu/activated carbon biofiltration. *Chemosphere* **2022**, *286*, 131686.
(69) Sun, Y.; Wang, T.; Han, C.; Lv, X.; Bai, L.; Sun, X.; Zhang, P. Facile synthesis of Fe-modified lignin-based biochar for ultra-fast adsorption of methylene blue: Selective adsorption and mechanism studies. *Bioresour. Technol.* **2022**, *344*, 126186.

https://doi.org/10.1021/acsomega.4c03496
ACS Omega 2024, 9, 30813−30825